Dalton Transactions

Accepted Manuscript

ROYAL SOCIETY OF CHEMISTRY

www.rsc.org/dalton

Journal Name

RSCPublishing

ARTICLE

Comprehending the effect of $MMoO_4$ (M = Co, Ni) nanoflakes on improving the electrochemical performance of NiO electrodes

Cite this: DOI: 10.1039/xoxxooooox

Received ooth January 2012,
Accepted ooth January 2012

DOI: 10.1039/xoxxooooox

www.rsc.org/

Lei An[a]†, Wenyao Li[a,b]†, Yunjiu Cao[a,c], Kaibing Xu[a], Rujia Zou[a,d] Tao Ji[a,c], Li Yu[a,e] and Junqing Hu[a]*

Design and fabrication of high performance supercapacitors with large specific capacitance and long lifespan still remain a challenge. We present two hydrothermal and another two annealing processes for the fabrication of hierarchical heterostructures of NiO@$MMoO_4$ (M = Co, Ni) nanosheet arrays on Ni foam. In this hierarchical structure, numerous $MMoO_4$ nanoflakes grow on a NiO nanosheet and the integration of $MMoO_4$ can improve the whole electrode's conductivity, leading an ideal pathway for electron and ion transport. The hierarchical NiO@$MMoO_4$ (M = Co, Ni) heterostructure electrode demonstrated remarkable electrochemical performance with high specific capacitance and predominant cycling stability, making it one of the perspective electrode materials for high performance supercapacitors.

Introduction

Because of their unique characteristics in terms of faster charge and discharge processes, long cycling life, high power density and great potency as power sources for applications in electric/hybrid electric vehicles and portable electronics, supercapacitors are widely considered to be one of the most perspective choices available for the rapid development of energy storage devices.[1-7] Although electric double-layer capacitors based on high surface area carbonaceous materials are widely used as commercial supercapacitors (SCs), pseudocapacitors with much higher specific capacitance, utilize fast and reversible surface or near surface reactions for charge storage, are competitive for high performance supercapacitors.[8-10]

Among various electrode nanomaterials, nickel oxide (NiO) has been widely investigated in supercapacitor applications due to its high theoretical capacitance (2584 F g^{-1}), environmental friendliness, low cost, high power density and good corrosion stability in alkaline solutions.[11-16] For instance, Zhang et al. fabricated NiO nano/microspheres via a refluxing approach with a specific capacitance of 525 F g^{-1} for supercapacitor electrode material at a current density of 4 A g^{-1}.[17] Chai et al. reported a specific capacitance of 340 F g^{-1} for flower-like NiO structures as an electrode material at a current density of 1 A g^{-1} via a facile hydrothermal and thermal decomposition process.[18] Tong et al. sythesized hierarchical NiO nanospheres via a facile trisodium citrate assisted precipitation route as an electrode material, which showed a specific capacitance of 603 F g^{-1} at 0.5 A g^{-1}.[19] However, most of the reported specific capacitances are still far below the theoretical values, as the single NiO materials possess poor electric conductivity and fail to support a fast electron transport.[20,21] Recently, an emerging concept of hierarchical hybrid heterostructures, such as metal/metal oxide,[22,23] metal oxide/conductive polymer,[24] metal oxide/metal oxide,[25-27] metal/semiconductor,[28] and semiconductor/metal oxide,[29] have been investigated due to their high versatility and applicability as indispensable components in supercapacitors. The heterostructured architecture can make full use of the advantages of both individuals and provide distinct characteristics through a combination or modification of each other. As an attractive member, $MMoO_4$ (M = Co, Ni) has attracted more and more research interest due to its excellent electrical conductivity and remarkable electrochemical energy storage performance resulting from the high electrical conductivity of the Mo element and the high electrochemical activity of the M ion (M = Co, Ni).[30-32] Nevertheless, the cycle performance of $NiMoO_4$ are still not very ideal,[33] and the specific capacity of $CoMoO_4$ remains to be further increased.[34] To meet the requirement of structural stability and higher specific capacitance, one promising route is to have meticulous design of nano-heterostructures and ingenious hybridization of bespoke pseudocapacitive materials with facile methods.

In this present work, we present a simple but powerful hydrothermal as well as annealing method to synthesize hierarchical heterostructures of NiO@$MMoO_4$ (M = Co, Ni) nanosheet arrays on nickel foam. The electrode materials directly grown on Ni foam can avoid the "dead" surface caused by conductive additives/polymer binders and a traditional miscellaneous slurry-coating process. Due to the unique properties of the unique heterostructures, such as good conductivity, porous features, robust mechanical strength,

shorter ion and electron transport path and direct growth on conductive substrates, hierarchical $NiO@MMoO_4$ microstructures exhibited high capacitance and excellent cycling stability when were studied systematically as electrodes for pseudocapacitors. The outstanding electrochemical performance will undoubtedly make the hybrid heterostructures attractive for high performance supercapacitors.

Experimental Characterization

All the chemicals were of analytical grade and used without further purification.

Synthesis of NiO nanosheet arrays

NiO nanosheet arrays were synthesized through combining a hydrothermal reaction and a thermal annealing process. In a typical synthetic procedure, a piece of nickel foam was carefully cleaned with 6 M HCl solution in an ultrasound bath for 30 min to remove the probable NiO layer on the surface and then washed by deionized water and absolute ethanol several times till to neutral. $Ni(NO_3)_2 \cdot 6H_2O$ (0.4 g), $CO(NH_2)_2$ (0.4 g) and NH_4F (HMT, 0.2 g) were dissolved into 50 mL deionized water. The above mixture was stirred for 30 min and followed transferred into a 60 mL polytetra-fluoroethylene (PTFE) (Tefion)-lined autoclave, and then a piece of cleaned nickel foam was immersed into the reaction solution. The autoclave was sealed and maintained at 110 ℃ for 8 h in an electric oven. After cooling to room temperature naturally, the products on Ni foam were carefully washed with deionized water and absolute ethanol and then dried at 70 ℃ overnight. Afterward, the samples were annealed at 350℃ for 2 h at a ramping rate of 2 ℃ min^{-1} to transform into NiO nanosheet arrays.

Preparation of hierarchical heterostructures of $NiO@MMoO_4$ (M = Co, Ni) nanosheet arrays

The self-supported NiO nanosheet arrays were used as the scaffold for $MMoO_4$ (M = Co, Ni) nanoflakes growth in the following hydrothermal technique and thermal annealing process. Concretely, 0.124g $Co(CH_3COO)_2 \cdot 4H_2O$ (or 0.118g $NiCl_2 \cdot 6H_2O$) and 0.121g $Na_2MoO_4 \cdot 2H_2O$ were dissolved in 50 ml deionized water and stirred for 30 min. Then, the mixed solution and Ni foam with NiO nanosheets were transferred into a 60 mL Tefion-lined autoclave, which was sealed and maintained at 150 ℃ for reasonable time. After being cooled down to room temperature, the products were collected and washed with deionized water and absolute ethanol, then dried at 50 ℃ for 4 h in air. Finally, the products were calcined at 350 ℃ with a ramping rate of 1 ℃ min^{-1} for 2 h to obtain heterostructures of $NiO@MMoO_4$ (M = Co, Ni) nanosheet arrays.

Characterization

X-ray diffraction (XRD) patterns of all the samples were recorded with a D/max-2550 PC X-ray diffractometer (XRD; Rigaku, Cu-Ka radiation). The morphology of the materials was examined with a scanning electron microscope (SEM; S-4800) and a transmission electron microscope (TEM; JEM-2010F) equipped with an energy dispersive X-ray spectrometer (EDX). The mass of the electrode materials was weighed on an XS analytical balance (Mettler Toledo; $\delta = 0.01$ mg).

Electrochemical measurement

Electrochemical measurements were performed on an Autolab Electrochemical Workstation (PGSTAT302N) using a three electrode electrochemical cell and 3 M KOH as the electrolyte. The Ni-foam-supported electroactive materials (~ 1 cm × 1 cm) were used directly as the working electrode. A saturated calomel electrode (SCE) was used as the reference electrode and a platinum (Pt) sheet electrode was used as the counter electrode. All potentials were referred to the reference electrode. The specific capacitance and current density were calculated based on the mass of the as-formed electroactive materials.

Results and discussion

The fabrication processes and the resulting novel electrode architectures developed in this work are schematically illustrated in Fig. 1. First, NiO nanosheet arrays were grown vertically on Ni-foam via a hydrothermal and annealing process. Ni-foam has been widely considered to be an ideal current collector for the controlled growth of electrode materials due to its uniform macropore structure (Fig. S1†), large supporting area and high electrical conductivity. The second is the controllable farbrication of $MMoO_4$ nanoflakes coating on the NiO nanosheet arrays through hydrothermal technique and thermal annealing process. In our design, the integration of $MMoO_4$ may contribute to the total capacitance because of the synergistic effect. We anticipate that such unique hybrid hierarchical microstructure would demonstrate superior electrochemical performance when used as an electrode for supercapacitors.

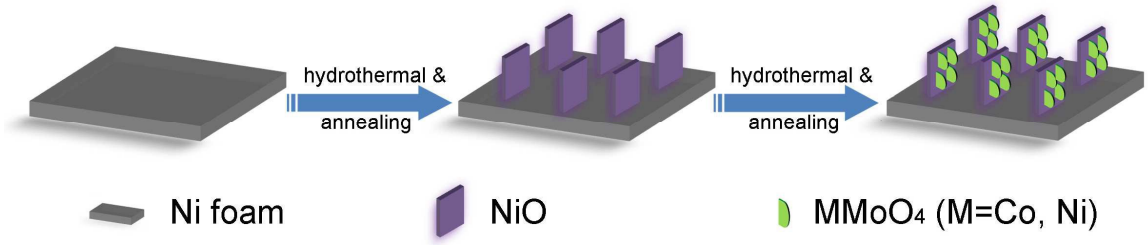

Fig. 1 Schematic illustration of the synthetic process of hierarchical $NiO@MMoO_4$ (M = Co, Ni) hybrid nanosheet arrays on Ni foam.

Journal Name RSCPublishing

ARTICLE

Scanning electron microscopy (SEM) and transmission electron microscopy (TEM) were employed to investigate the morphology and structure of the as-synthesized materials. Shown in Fig. 2a is a low magnification SEM image of NiO nanosheets, which were fully and uniformly grown on each strip of the Ni-foam with high density. Higher magnification SEM images (Fig. 2b, c) exhibit that the NiO nanosheets have an intercross-linked character, forming an ordered and 3D network with reasonable open space. A typical TEM image (Fig. 2d) shows that the as-grown nanosheets are full of porous structures and the pore sizes are about several nanometers. The formation of the pores could be caused by H_2O and gas release during the decomposition/oxidation of the intermediates during thermal annealing. Such electrode materials with numerous pores in the NiO nanosheets and highly ordered arrays with considerable intervals among them is beneficial to ion diffusion and charge transport. The corresponding selected-area electron diffraction (SAED) pattern (Fig S2†) of the microstructure demonstrates that the as-synthesized sample has polycrystalline nature. Fig. 2e is a high-resolution TEM image (HRTEM) of a NiO nanosheet, exhibiting the d-spacing of 0.148 nm corresponding to the distance of the {220} planes of the NiO crystal. In our study, we have carefully examined the whole area of this nanosheet by HRTEM imaging without rectifying the sample in any way. All taken HRTEM images revealed the same lattice fringe characteristics exactly of the NiO crystal, indicating the as-sythesized NiO nanosheet with a nature of single crystal. To better understand the chemical composition of the as-prepared product, the energy dispersive X-ray (EDX) spectrometry characterization of the mesoporous NiO was also conducted. In Fig. 2f, it was found that the nanosheet consists of Ni, O, Cu and C elements, in which the Cu peaks were derived from the Cu grid and the C element resulted from C membranes on the Cu grid, revealing the formation of NiO material.

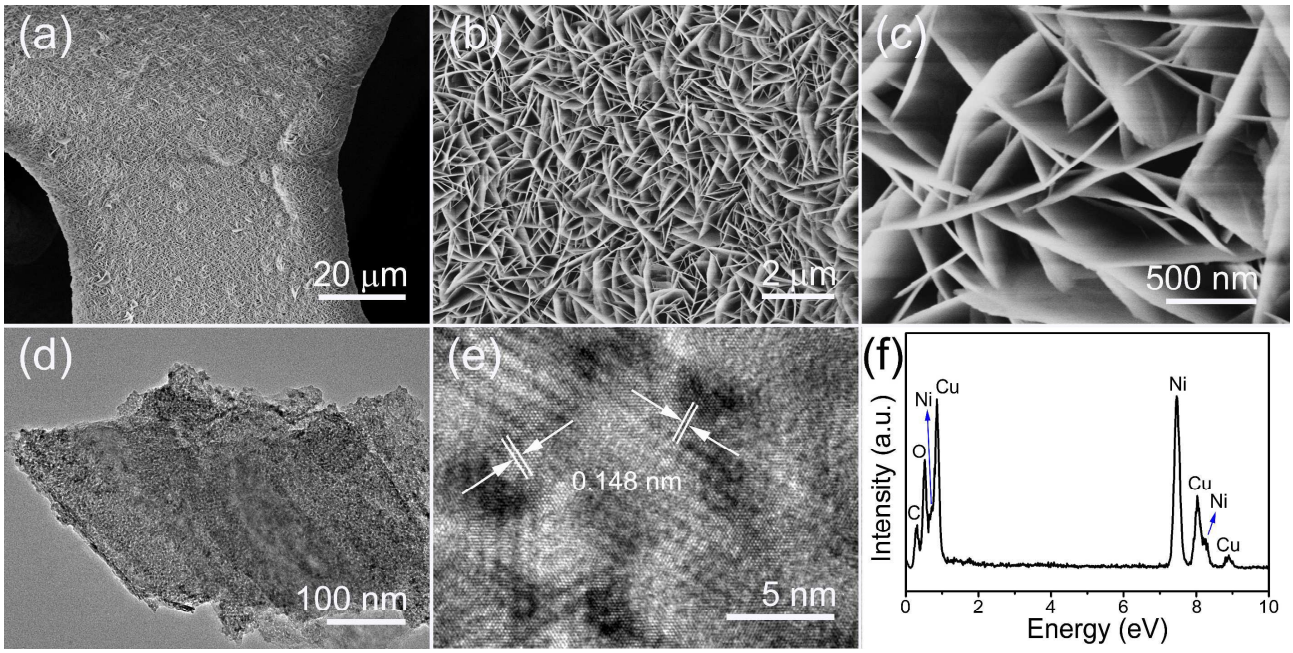

Fig. 2 (a-c) Different magnification SEM images of the NiO nanosheet arrays on Ni foam. (d, e) TEM and HRTEM images of a NiO nanosheet, respectively. (f) EDX pattern of the NiO nanosheets scratched from Ni foam.

The interconnected mesoporous NiO nanosheet arrays uniformly grown on the Ni-foam can serve as an ideal scaffold for loading additional electroactive pseudocapacitive materials, and thus can improve the electrochemical performance. In our work, two of well-known transition metal compounds, $CoMoO_4$ and $NiMoO_4$ nanoflakes, were coated onto mesoporous NiO nanosheet arrays via hydrothermal technique. In a control, $CoMoO_4$ and $NiMoO_4$ nanoflakes were also grown on Ni foam using the same methods without NiO material (Fig S3 †). Shown in Fig. 3a, b are low- and high- magnification SEM images of $CoMoO_4$ nanoflakes grown on porous NiO nanosheet arrays. These $CoMoO_4$ nanosheets were grown vertically on the double sides of the NiO nanosheets, occupying considerable intervals between two adjoining walls, assembling into

interesting 3D hierarchical NiO@$CoMoO_4$ nanosheet array heterostructures. Each nanoflake displays a thickness variation of 10-30 nm along its height of ~ 200 nm. Fig. 3c is a TEM image taken from the NiO@$CoMoO_4$ nanosheet detached from Ni foam, revealing that the thickness of the as-synthesized $CoMoO_4$ nanoflakes is ~ 20 nm, which is consistent with the SEM results. Fig. 3d, e demonstrated that $NiMoO_4$ nanoflakes were uniformly grown on the NiO nanosheets. The fluffy $NiMoO_4$ nanoflakes coated uniformly on the NiO nanosheets, forming an unique 3D hierarchical NiO@$NiMoO_4$ microstructure, which can also be verified through a TEM image taken from the NiO@$NiMoO_4$ nanosheet detached from Ni foam (Fig 3f), while each $CoMoO_4$ sheet is as thin as 2-5 nm (Fig S4†). Notably, the integration of $MMoO_4$ (M = Co, Ni) into the arrays does not deteriorate the ordered structure and such unique heterostructures assembled by combining porous NiO nanosheets with thin $MMoO_4$ nanoflakes will have a larger electroactive sites but not preventing contact between the NiO nonosheets and ions in the electrolyte. Thus, superior electrochemical performance based on the unique heteroarchitectures can be expected.

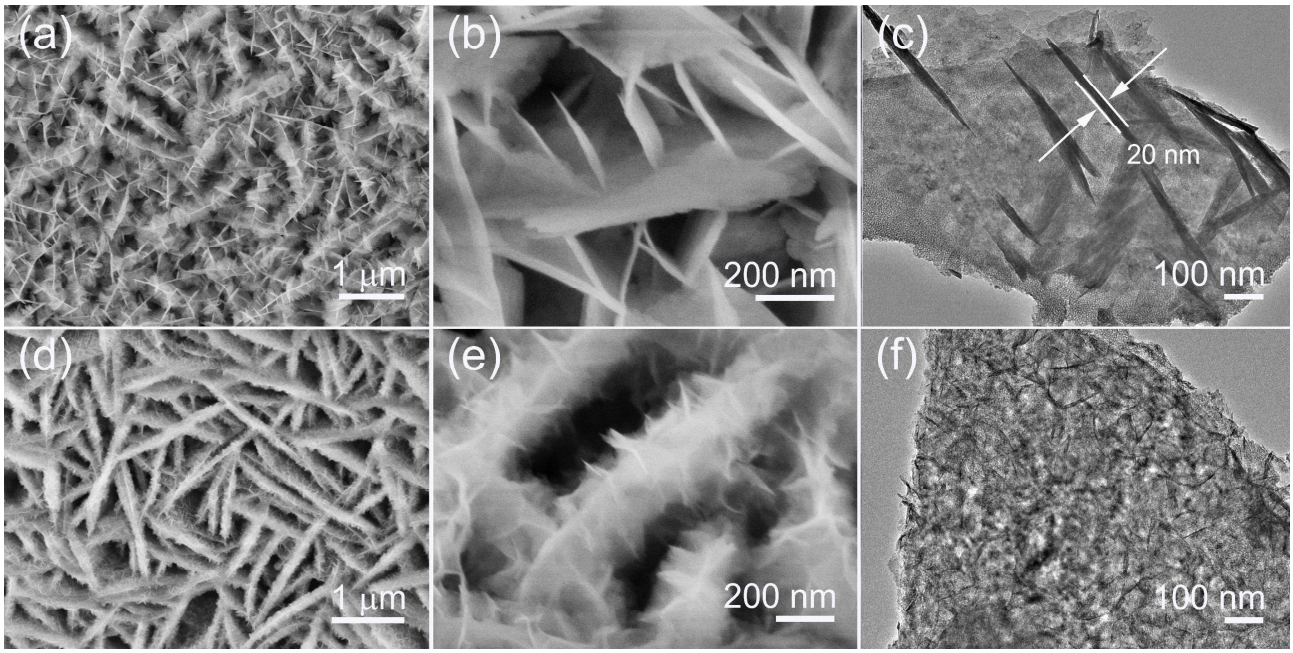

Fig. 3 SEM and TEM images of the hierarchical NiO@$CoMoO_4$ hybrid composites after 1.5 h of hydrothermal reaction (a-c) and the NiO@$NiMoO_4$ hybrid heterostructures after 2 h of hydrothermal reaction (d-f), respectively.

The XRD patterns of NiO@$MMoO_4$ (M = Co, Ni) hybrid hererostructures on Ni foam were shown in Fig. S5†, NiO peaks of (111), (200), (220) and (311) were observed in the XRD pattern of both NiO@$CoMoO_4$ and NiO@$NiMoO_4$ hererostructures, in accordance with the reported data (JCPDS card no. 47-1049). In addition, the signals of both $CoMoO_4$ and $NiMoO_4$ peaks also can be found in their XRD patterns, respectively. However, their peaks cannot be distinguished very clearly from the mixed signals of NiO, $MMoO_4$ and Ni foam, which could be attributed to the low crystallinity of the $MMoO_4$ (M = Co, Ni) nanoflakes[35-38] as well as the strong impact of Ni foam. Therefore, in order to understand the chemical composition of the as-prepared products better, the energy dispersive X-ray (EDX) spectrometry characterizations of the NiO@$MMoO_4$ composites were also conducted. The EDX spectrum of NiO@$CoMoO_4$ (Fig. S6a†) indicates that apart from Ni and O, Co and Mo also can be detected in the hybrid composites, which should be attributed to the presence of $CoMoO_4$. Similarly, the EDX spectrum of NiO@$NiMoO_4$ (Fig. S6b†) indicates that apart from Ni and O, Mo also can be detected in the hybrid composites, which should be attributed to the presence of $NiMoO_4$. In both EDX patterns, the Cu and C signals come from the TEM grid.

To reveal the growth mechanism of the $CoMoO_4$ and $NiMoO_4$ nanoflakes rooted on the surface of NiO nanosheets, the SEM images based on different hydrothermal reaction times were taken. The morphology evolution of the NiO@$CoMoO_4$ and NiO@$NiMoO_4$ hybrid heterostructures was shown in Fig. 4 and Fig. S7†, respectively. When putting the Ni foam containing NiO nanosheets arrays into the autoclave, many $CoMoO_4$ precursor nuclei appear on the surface of the NiO nanosheets. After the initial 0.5 h reaction, the SEM image, Fig. 5a, shows the smooth NiO sheet surface becoming rough and decorated by smaller $CoMoO_4$ precursor "sprouts", indicating that the $CoMoO_4$ precursor is beginning to grow on the surface of NiO nanosheets. With the hydrothermal reaction time prolonged to 1.5 h (Fig. 4b), many $CoMoO_4$ precursor transformed from "sprouts" to nanosheets, uniformly covered on the surface of NiO nanosheets, exhibiting a unique feature with reasonable intervals among neighboring nanounits. Prolonging the reaction time to 3 h, the surface of the $CoMoO_4$ precursor nanoflakes became larger and dense (Fig. 4c). Further increasing the

reaction time to 6 h, the nanoflakes got extremely dense and larger and cover the NiO nanosheet arrays completely (Fig. 4d). Besides, many new nucleis appeared on the surface of the dense $CoMoO_4$ precursor nanosheets. Note that much more $CoMoO_4$ grown on the surface of NiO nanosheets may hinder the ion diffusion to NiO electrode materials. Besides, The morphology evolution of the $NiO@NiMoO_4$ is similar to that of $NiO@CoMoO_4$ hybrid heterostructures, as shown in Fig. S7†. Therefore, the variation of the electrochemical performance of the $NiO@CoMoO_4$ and $NiO@NiMoO_4$ electrodes with different hydrothermal reaction time need to be examined in the following work.

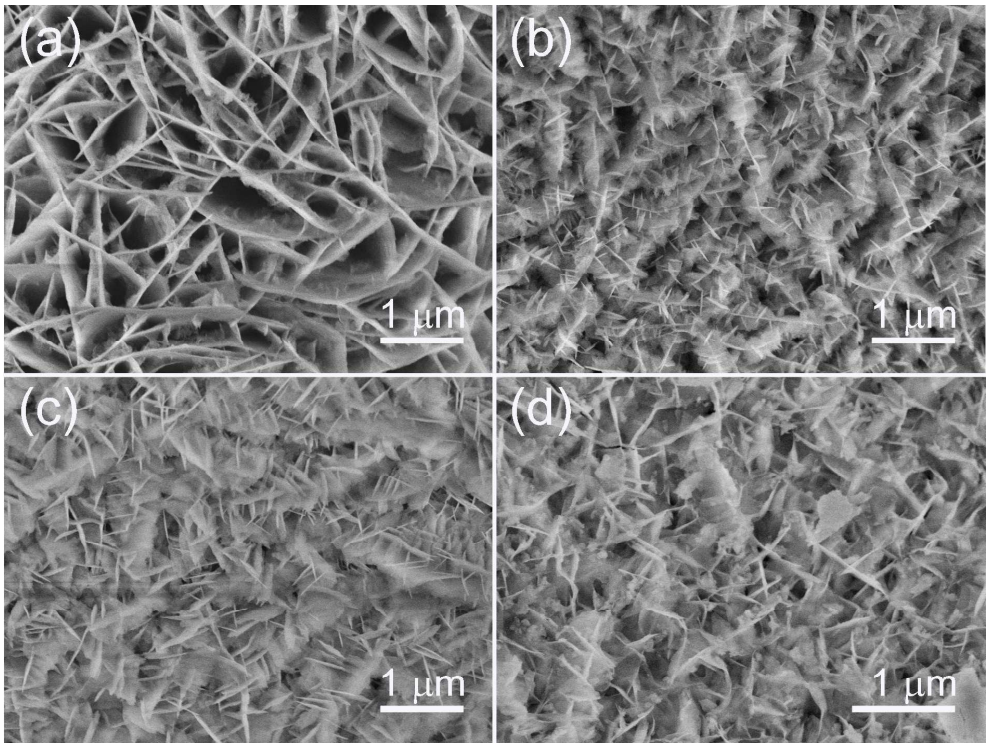

Fig. 4 SEM images of the morphology evolution of the hierarchical $NiO@CoMoO_4$ heterostructures obtained at different hydrothermal stages: (a) 0.5 h, (b) 1.5 h, (c) 3 h, and (d) 6 h.

Then, the electrochemical properties of the $NiO@MMoO_4$ electrodes were investigated in a three-electrode cell with 3 M KOH aqueous solution as the electrolyte. To choose the optimal electrodes of $NiO@MMoO_4$ (M = Co, Ni), both the variation of the specific capacitance of the $NiO@CoMoO_4$ and $NiO@NiMoO_4$ electrodes with different reaction time were investigated. Shown in Fig. 5a, c demonstrated a direct comparison of the galvanostatic charge-discharge curves of $NiO@MMoO_4$ (M = Co, Ni) electrode at a current density of 4 A/g at different reaction time. Fig. 5b, d exhibited specific capacitance of the $NiO@MMoO_4$ electrode as a function of the $MMoO_4$ hydrothermal time based on charge-discharge curves. Obviously, $NiO@CoMoO_4$ with 1.5 h and $NiO@NiMoO_4$ with 2 h were chosen to be the optimum electrodes for the following electrochemical tests due to their larger specific capacitance, comparing with their corresponding electrodes in other different reaction time.

Journal Name RSCPublishing

ARTICLE

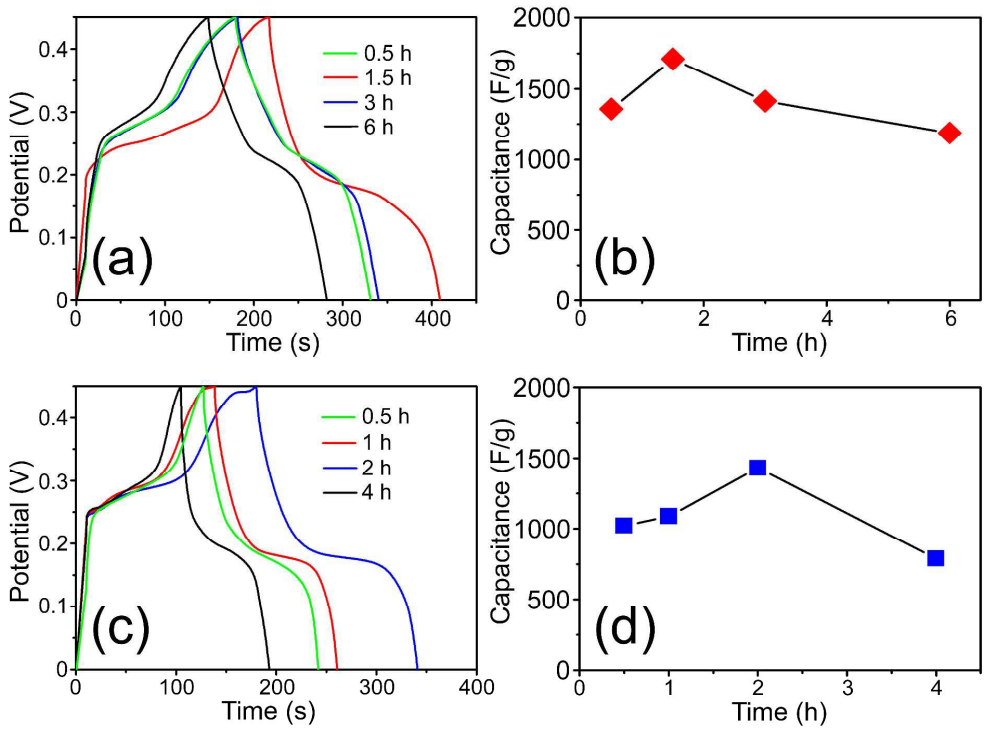

Fig. 5 (a) Galvanostatic charge-discharge curves and (b) specific capacitance of the NiO@$CoMoO_4$ nanosheet hybrid electrode as a function of the $CoMoO_4$ nanoflakes grown via a different hydrothermal time, respectively. (c) Galvanostatic charge-discharge curves and (d) specific capacitance of the NiO@$NiMoO_4$ nanosheet hybrid electrode as a function of the $NiMoO_4$ nanoflakes grown via a different hydrothermal time, respectively.

Fig. 6a shows the cyclic voltammogram (CV) curves of NiO@$CoMoO_4$, NiO@$NiMoO_4$ hybrid composites, NiO, $NiMoO_4$, $CoMoO_4$ nanosheets electrodes at a scan rate of 50 mV s^{-1} in a potential window of -0.2 to 0.6 V. Obviously, the enclosed areas of both the NiO@$CoMoO_4$ and NiO@$NiMoO_4$ electrodes are much larger than that of the NiO, $NiMoO_4$, $CoMoO_4$ electrodes, indicating substantial improvement of the specific capacitance of the as-formed hierarchical heterostructures after coating $MMoO_4$ (M = Co, Ni). First, the accession of $MMoO_4$ can enlarge the total electroactive sites and make active materials fully access the KOH electrolyte, allowing for easy diffusion of the electrolyte into the inner region of the electrodes. Second, the $MMoO_4$ electrode materials would contribute to additional pseudocapacitance in alkaline solution and a material-combination will provide multifunctional and synergistic effects. Moreover, the integrated CV area for the Ni-foam electrode is negligible as compared with that of the NiO, $NiMoO_4$, $CoMoO_4$ and NiO@$MMoO_4$ electrodes, and thus the influence on the performance of the electrodes can be ignored in our work. Fig. 6a and Fig. S8a† show the typical cyclic voltammetry (CV) curves of NiO@$CoMoO_4$ and NiO@$NiMoO_4$ nanocomposites at different scan rates ranging from 5 to 100 mV s^{-1}, respectively. A pair of redox peaks is visible in each CV curve, which are mainly resulted from redox reactions related to M-O/M-O-OH, where M represents Ni or Co ions,[9,32,39] indicating the pseudocapacitive nature of the as-prepared hierarchical heterostructure electrode materials. Interestingly, the redox current increased along with the extending of scan rate. Besides, the oxidation and reduction peaks shifted toward higher and lower potential, respectively, with a large potential separation. The shift of the oxidation/reduction peaks may ascribe to the increment of the internal diffusion resistance in the electrode materials.[40-41] Furthermore, the shapes of these CV curves show almost no significant change as the scan rate increases from 5 to 100 mV s^{-1}, suggesting a good capacitive behavior of the heterostructure electrode materials. Similar phenomenons also were observed in their corresponding individual component electrodes (Fig. S8b-d †). Shown in Fig. 6c is a direct comparison of the charge-discharge curves of the five electrode

materials at a current density of 4 A g^{-1}. It can be seen that the charge curves are not strictly but approximately symmetric to their corresponding discharge counterparts, indicating their good reversibility. It is worthy to note that the specific capacitance of the NiO@$CoMoO_4$ and NiO@$NiMoO_4$ electrodes can reach 1711 F g^{-1} and 1431 F g^{-1}, respectively, which are higher than that of the NiO (1022 F g^{-1}), $CoMoO_4$ (684 F g^{-1}) and $NiMoO_4$ (787 F g^{-1}) nanosheet electrodes. Further galvanostatic CD investigations of the five electrode materials between 0 and 0.45 V at different current densities are shown in Fig. 6d and S9†. The specific capacitances of both NiO@$CoMoO_4$ and NiO@$NiMoO_4$ electrodes were also higher than those of their corresponding three kind of individual component electrode materials at each current density. The calculated specific capacitance as a function of the discharge current density is plotted in Fig. 6e. It is worth mentioning that the highest specific capacitance of the NiO@$CoMoO_4$ and NiO@$NiMoO_4$ electrodes can reach 1834 and 1685 F g^{-1} at 2.4 A g^{-1}, respectively, which are higher than those of the individual component nanosheets (872 F g^{-1} for $CoMoO_4$, 979 F g^{-1} for $NiMoO_4$ and 1099 F g^{-1} for NiO at the same current density). Besides, The performance of the hierarchical NiO@$MMoO_4$ heterostructures also are remarkable compared with other reported NiO or $MMoO_4$ (M = Co, Ni) based electrode materials in previous literature, as summarized in Table S1. † The specific capacitance of the hierarchical NiO@$MMoO_4$ heterostructures are higher than those of the reported electrode materials,[17-19, 42-48] which should contribute to synergistic and multifunctional effects derived from the unique material-combination and hierarchical heteroarchitecture. Energy density and power density are the two vital parameters for evaluating the electrochemical applications of supercapacitors. Ragone plots of the NiO@$MMoO_4$ (M = Co, Ni) hierarchical heterostructures and the NiO, $CoMoO_4$ and $NiMoO_4$ nanosheets are shown in Fig. 6f. At a power density of 540 W kg^{-1}, the NiO@$CoMoO_4$ and NiO@$NiMoO_4$ electrode materials can deliver an energy density as high as 51.6 and 47.4 Wh kg^{-1}, respectively, which are larger than that of the $CoMoO_4$ nanosheets (24.5 Wh kg^{-1}), $NiMoO_4$ nanosheets (27.5 Wh kg^{-1}) and NiO nanosheets (30.9 Wh kg^{-1}) electrodes. Significantly, the energy density of the prepared electrode from the hierarchical NiO@$MMoO_4$ (M = Co, Ni) heterostructures are larger than those of the reported nanostructured Ni- or Co- based electrodes, such as hierarchical NiO nanospheres (13.4 Wh kg^{-1}),[19] rGO-supported $CoMoO_4$ nanorods (14.1 Wh kg^{-1}),[42] $NiMoO_4$ nanotubes (24.3 Wh kg^{-1}),[44] and NiO@C hollow hybrid networks (19.9 Wh kg^{-1}).[49]

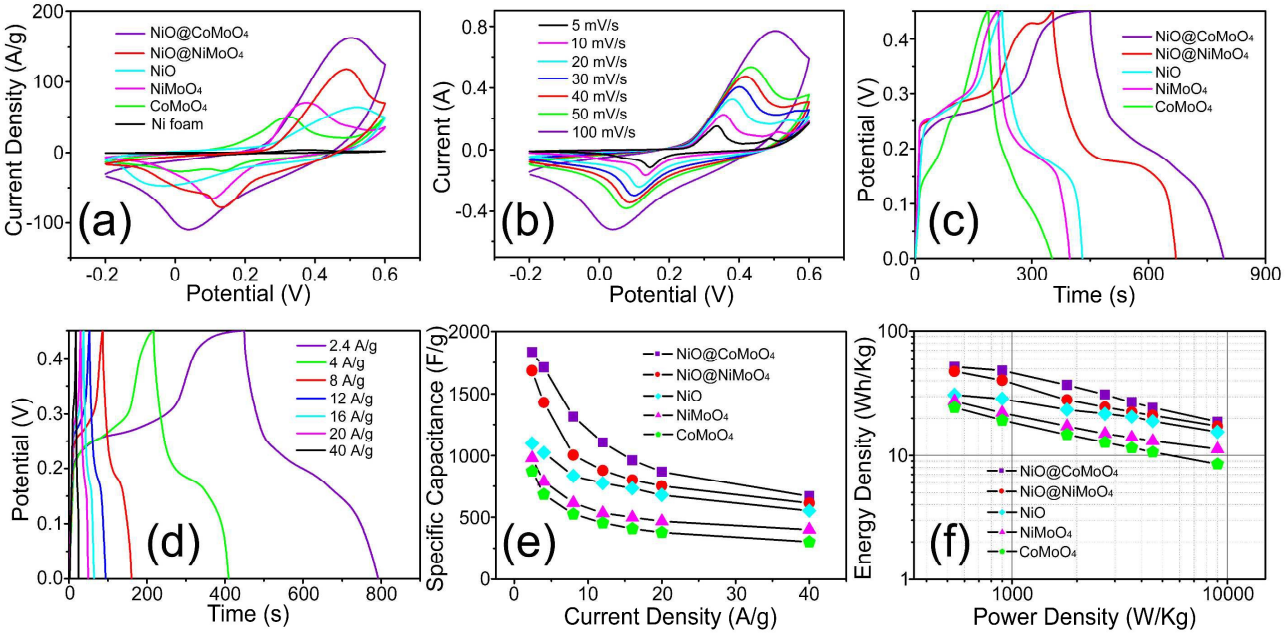

Fig. 6 (a) CV curves at a scan rate of 50 mV s^{-1} of the NiO@$MMoO_4$ (M = Co, Ni) hybrid composites, NiO, $MMoO_4$ (M = Co, Ni) nanosheets and Ni foam electrodes, respectively. (b) CV curves of the hierarchical NiO@$CoMoO_4$ microstructure as an electrode at different scan rates ranging from 5 to 100 mV s^{-1}. (c) Galvanostatic charge-discharge curves at a current density of 2.4 A g^{-1} of the NiO@$MMoO_4$ (M = Co, Ni) hybrid composites, NiO and $MMoO_4$ (M = Co, Ni) nanosheets, respectively. (d) Galvanostatic charge-discharge curves of the NiO@$CoMoO_4$ electrode at different current densities ranging from 2.4 to 40 A g^{-1}. (e) Specific capacitance at different current densities and (f) Ragone plot (energy density vs. power density) of the NiO@$MMoO_4$ (M = Co, Ni) hybrid composites, NiO and $MMoO_4$ (M = Co, Ni) nanosheets, respectively.

Cycling performance is a critical aspect in determining the supercapacitors for many practical applications. The cycling performance of the NiO@$MMoO_4$ (M = Co, Ni) were conducted at a scan rate of 50 mV s^{-1} for 3000 cycles, as shown in Fig. 7a. The capacitance of both NiO@$CoMoO_4$ and NiO@$NiMoO_4$ electrodes almost have no change and the final

specific capacitance can remain as high as 103.5 % and 98.2% of their corresponding initial capacitance after 3000 cycles, respectively. Insets in Fig. 7a exhibit their corresponding 1st and the 3000th CV curves of at a scan rate of 50 mV s^{-1}. The shape and enclosed areas (after 3000 cycle) of both NiO@$CoMoO_4$ and NiO@$NiMoO_4$ have teeny changes compared with their corresponding 1st cycling curve, indicating stable electrochemical performance of the hierarchical heteroarchitectures. Besides, the capacitance retention of the NiO@$MMoO_4$ (M = Co, Ni) hybrid composites are better than other reported Ni- or Co- based results, such as hierarchical Mo-decorated Co_3O_4 nanowire arrays (53 % capacitance retention after 2000 cycles),[35] $NiMoO_4$ nanospheres (74.5 % capacitance retention after 2000 cycles)[45] and nano β-$NiMoO_4$-$CoMoO_4$•xH_2O composites (78 % capacitance retention after 500 cycles).[50] To further understand the influence of $MMoO_4$ (M = Co, Ni) nanoflakes on the NiO electrode, we studied the internal resistance of the NiO and NiO@$MMoO_4$ (M = Co, Ni) electrodes. Shown in Fig. 7b are the iR drop (where i and R represent the current and resistance, respectively) of the NiO@$MMoO_4$ (M = Co, Ni) and NiO electrodes as a function of current density. The iR drop was resulting from the discharge curves obtained at different current densities ranging from 2.4 to 40 A g^{-1}. Apparently, both NiO@$CoMoO_4$ and NiO@$NiMoO_4$ electrodes demonstrate much smaller internal resistance than the NiO electrode depend on the slopes of the iR drop plots, indicating that the integration of both $CoMoO_4$ and $NiMoO_4$ nanoflakes can improve the conductivity of the whole electrode, which is also further confirmed by the following electrochemical impedance spectroscopy (EIS) tests. Results of EIS patterns on the NiO@$MMoO_4$ (M = Co, Ni) hierarchical heterostructures and NiO electrodes are shown in Fig. 7c. As can be seen, all the impedance curves are similar in form, with a semicircle at high frequency and a linear component at low frequency region. Noticeably, the slope of the straight line in the low frequency region of NiO@$MMoO_4$ (M = Co, Ni) inclined at an angle of nearly 90° to the Z' axis compared with that of NiO eletrode, suggesting a more superior electrochemical capacitive behavior in the NiO@$MMoO_4$ electrodes. NiO@$MMoO_4$ (M = Co, Ni) and NiO electrodes can be fitted in the same equivalent fitting circuit shown in Fig. 7d, in which R_s is the internal resistance, R_{ct} is the Faradaic interfacial charge-transfer resistance, CPE represents the constant phase element accounting for a double-layer capacitance, C_F is the Faradaic pseudocapacitor and W is the Warburg impedance, the result of the frequency dependence of ion diffusion from the electrolyte solution to the electrode interface, corresponding to the slope of the straight line in low frequency range. The R_s value of both NiO@$CoMoO_4$ (0.289 Ω) and NiO@$NiMoO_4$ electrodes (0.3 Ω) were lower than that of the NiO electrode (0.453 Ω). In addition, the NiO electrode have a larger charge transfer resistance (R_{ct}) value (5.2 Ω) than that of NiO@$CoMoO_4$ (1.39 Ω) and NiO@$NiMoO_4$ (3.72 Ω), which demonstrates that integration of $MMoO_4$ (M = Co, Ni) nanoflakes can improve the whole electrode's conductivity and the unique microstructure can provide an ideal pathway for electron and ion transport without kinetic limitations. It is worth mentioning that the as-fitted equivalent circuits have higher accuracy due to the as-gained fitting curves of the three electrodes can match with their corresponding original testing impedance curves very well, as shown in Fig. 7 e1-e3.

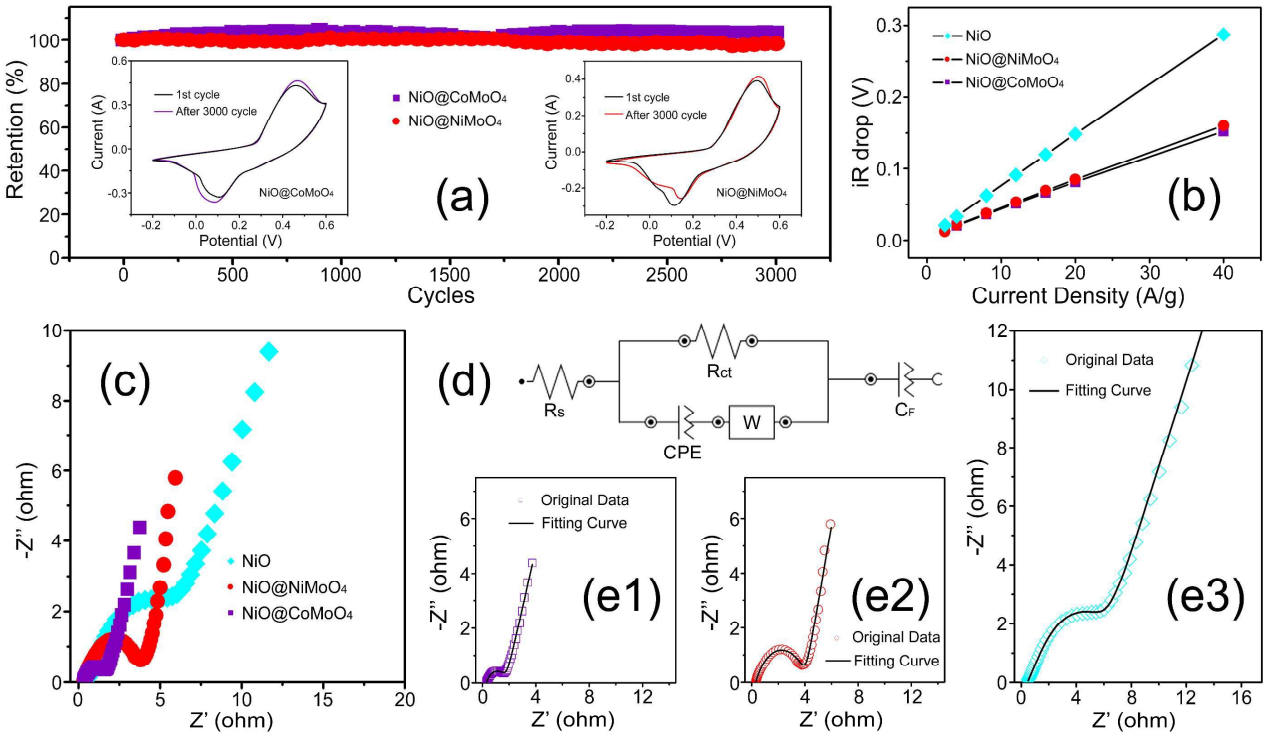

Fig 7 (a) Cycling performance of the $NiO@CoMoO_4$, $NiO@NiMoO_4$ hybrid composites recorded at a scan rate of 50 mV s^{-1} for 3000 cycles, respectively; insets are their corresponding CV profiles of the 1st and 3000th cycles, respectively. (b) iR drop measured at different current densities, (c) EIS spectra comparison, (d) equivalent fitting circuit, (e1-e3) fitting curves of the $NiO@CoMoO_4$, $NiO@NiMoO_4$ and NiO electrodes, respectively.

The electrochemical measurement demonstrates that hierarchical $NiO@MMoO_4$ (M = Co, Ni) heterostructures delivers outstanding specific capacitance as well as excellent cycling stability. The remarkable electrochemical performance could be derived from the following structural features. First, the $NiO@MMoO_4$ (M = Co, Ni) hierarchical heterostructures directly grown on the Ni foam (conductive substrate) could avoid "dead" volume caused by the cumbersome process of mixing active materials with polymer binder/conductive additives. Second, the porous feature of the NiO nanosheets largely increases the amount of electroactive sites. Third, both NiO and $MMoO_4$ (M = Co, Ni) are good pseudocapacitive materials and the reasonable material-combination will provide multifunctional and synergistic effects. In addition, the integration of $MMoO_4$ (M = Co, Ni) nanoflakes can improve the whole electrode's conductivity, leading an ideal pathway for electron and ion transport in the unique hierarchical heterostructures. Compared with the $NiO@NiMoO_4$ electrode, it can be clearly seen that the $NiO@CoMoO_4$ product exhibited better electrochemical performance with both higher capacitance and better cycling stability. This might be understood concerned the following factors. The $NiMoO_4$ nanoflakes surround and fully cover the entire mesoporous NiO nanosheets, which may cause some pores of NiO nanosheets were covered, leading the decrease of electroactive sites compared with that of $CoMoO_4$ nanoflakes, grown on the surface of the NiO nanosheets vertically. In addition, the integration of $CoMoO_4$ nanoflakes may improve the whole electrode's conductivity more significantly compared with that of $NiMoO_4$ nanoflakes, which can be verified by the smaller values of internal resistance (R_s) and Faradaic interfacial charge-transfer resistance (R_{ct}) of the $NiO@CoMoO_4$ electrode in the EIS analysis mentioned in Fig. 7.

Conclusions

The tailored hierarchical $NiO@MMoO_4$ (M = Co, Ni) heterostructures were synthesized through a facile and powerful hydrothermal and annealing method. With this unique architecture, each component offers an essential function for energy storage, which could be the most important factor in understanding the synergetic effect between NiO and $MMoO_4$ (M = Co, Ni). Both the synthesized 3D hierarchical $NiO@CoMoO_4$ and $NiO@NiMoO_4$ hybrid composite electrodes exhibited favorable electrochemical performance, with high specific capacitance of 1834 and 1685 F g^{-1} at 2.4 A g^{-1} and good cycling stability of 103. 5 % and 98.2 % of their corresponding initial specific capacitance after 3000 cycles, respectively. Thus, the $NiO@MMoO_4$ (M = Co, Ni) electrodes with outstanding electrochemical performance should be considered as perspective materials for high-performance supercapacitors.

Acknowledgements

This work was financially supported by the National Natural Science Foundation of China (Grants 21171035, 51302035, 51472049, and 11204030), the Ph.D. Programs Foundation of the Ministry of Education of China (Grants 20110075110008 and 20130075120001), the National 863 Program of China (Grant 2013AA031903), and the Fundamental Research Funds for the Central Universities. The Key Grant Project of Chinese Ministry of Education (Grant 313015), the Science and Technology Commission of Shanghai Municipality (Grant 13ZR1451200), the Program Innovative Research Team in University (Grant IRT1221), the Hong Kong Scholars Program, the Shanghai Leading Academic Discipline Project (Grant B603), and the Program of Introducing Talents of Discipline to Universities (Grant 111-2-04)

Notes and references

[a] State Key Laboratory for Modification of Chemical Fibers and Polymer Materials, College of Materials Science and Engineering, Donghua University, Shanghai 201620, China.
[b] School of Material Engineering, Shanghai University of Engineering Science, Shanghai 201620, China.
[c] School of Fundamental Studies, Shanghai University of Engineering Science, Shanghai 201620, China.
[d] Center of Super-Diamond and Advanced Films (COSDAF), Department of Physics and Materials Science, City University of Hong Kong, Hong Kong.
[e] Ian Wark Research Institute, University of South Australia, Mawson Lakes, SA 5095, Australia.

E-mail: hu.junqing@dhu.edu.cn.
† These authors contributed equally to the work.
Electronic Supplementary Information (ESI) available. See DOI: 10.1039/b000000x/

1 S. Chabi, C. Peng, D. Hu and Y. Q. Zhu, *Adv. Mater.,* 2014, **26**, 2440.
2 Z. Q. Niu, H. B. Dong, B. W. Zhu, J. Z. Li, H. H. Hng, W. Y. Zhou, X. D. Chen and S. S. Xie, *Adv. Mater.*, 2013, **25**, 1058
3 C. G. Hu, L. Song, Z. P. Zhang, N. Chen, Z. H. Feng and L. T. Qu, *Energy Environ. Sci.*, 2015, 8, 31.
4 G. Nystrom, A. Marais, E. Karabulut, L. Wagberg, Y. Cui and M. M. Hamedi, *Nat. Commun.*, 2015, 6, 7259.
5 Y. Zhang, W. Y. Bai, X. L. Cheng, J. Ren, W. Weng, P. N. Chen, X. Fang, Z. T. Zhang and H. S. Peng, *Angew. Chem. Int. Ed.*, 2014, 53, 14564.
6 J. R. Miller and P. Simon, *Science*, 2008, 321, 651.
7 X. Ge, C. D. Gu, Y. Lu, X. L. Wang and J. P. Tu, *J. Mater. Chem. A*, 2013, 1, 13454.
8 C. Liu, F. Li, L. P. Ma and H. M. Cheng, *Adv. Mater.*, 2010, 22, 28.
9 S. J. Peng , L. L. Li , H. B. Wu , S. Madhavi and X. W. Lou. *Adv. Energy Mater.*, 2015, 5, 1401172.
10 H. B. Li, M. H. Yu, F. X. Wang, P. Liu, Y. Liang, J. Xiao, C. X. Wang, Y. X. Tong and G. W. Yang, *Nat. Commun.*, 2013, 4, 1894.

11 Z. H. Yang, F. F. Xu, W. X. Zhang, Z. S. Mei, B. Pei and X. Zhu, *J. Power Sources*, 2014, 246, 24.
12 L. An, K. B. Xu, W. Y. Li, Q. Liu, B. Li, R. J. Zou, Z. G. Chen and J. Q. Hu, *J. Mater. Chem. A*, 2014, 2, 12799.
13 F. Luan, G. Wang, Y. Ling, X. Lu, H. Wang, Y. Tong, X. X. Liu, Y. Li, *Nanoscale*, 2013, 5, 7984.
14 K. Liu and M. A. Anderson, *J. Electrochem. Soc.*, 1996, 14, 124.
15 X. J. Zhang, W. H. Shi, J. X. Zhu, W. Y. Zhao, J. Ma, S. Mhaisalkar, T. L. Maria, Y. H. Yang, H. Zhang, H. H. Hng and Q. Y. Yan, *Nano Res.*, 2010, 3, 643.
16 M. L. Huang; C. D. Gu; X. Ge; X. L. Wang and J. P. Tu, *J. Power Sources*, 2014, 259, 98.
17 C. Z. Yuan, X. G. Zhang, L. H. Su, B. Gao and L. F. Shen, *J. Mater. Chem.*, 2009, 19, 5772.
18 H. Chai, X. Chen, D. Z. Jia, S. J. Bao and W. Y. Zhou, *Mater. Res. Bull.*, 2012, 47, 3947.
19 D. D. Han, P. C. Xu, X. Y. Jing, J. Wang, P. P. Yang, Q. H. Shen, J. Y. Liu, D. L. Song, Z. Gao and M. L. Zhang, *J. Power Sources*, 2013, 235, 45.
20 S. K. Meher, P. Justin and G. R. Rao, *ACS Appl. Mater. Interfaces*, 2011, 3, 2063.
21 M. Huang, F. Li, J. Y. Ji, Y. X. Zhang, X. L. Zhao and X. Gao, *CrystEngComm*, 2014, 16, 2878.
22 S. S. Gu, Z. Lou, X. D. Ma and G. Z. Shen, *ChemElectroChem*, 2015, 2, 1042.
23 T. F. Qiu, B. Luo, M. Giersig, E. M. Akinoglu, L. Hao, X. J. Wang, L. Shi, M. H. Jin and L. J. Zhi, *Small*, 2014, 10, 4136.
24 C. Choi, S. H. Kim, H. J. Sim, J. A. Lee, A. Y. Choi, Y. T. Kim, X. Lepro, G. M. Spinks, R. H. Baughman and S. J. Kim, *Sci. Rep.*, 2015, 5, 9387.
25 Y. Jiao, Y. Liu, B. S. Yin, S. W. Zhang, F. Y. Qu and X. Wu, *Nano Energy*, 2014, 10, 90.
26 M. Huang, Y. X. Zhang, F. Li, Z. C. Wang, Alamusi, N. Hu, Z. Y. Wen and Q. Liu, *Sci. Rep.*, 2014, 4, 4518.
27 X. H. Xia, J. P. Tu, Y. Q. Zhang, X. L. Wang, C. D. Gu, X. B. Zhao and H. J. Fan, *ACS Nano*, 2015, 6, 5531.
28 P. C. Chen, S. J. Hsieh, J. Zou and C. C. Chen, *Mater. Lett.*, 2014, 133, 175.
29 J. B. Wu, R, Q. Guo, X. H. Huang and Y. Lin, *J. Power Sources*, 2013, 243, 317.
30 J. Haetge, I. Djerdj and T. Brezesinski, *Chem. Commun.*, 2012, 48, 6726.
31 M. C. Liu, L. B. Kong, X. J. Ma, C. Lu, X. M. Li, Y. C. Luo and L. Kang, *New J. Chem.*, 2012, 36, 1713.
32 W. Xiao, J. S. Chen, C. M. Li, R. Xu and X. W. Lou, *Chem. Mater.*, 2010, 22, 746.
33 M. C. Liu, L. Kang, L. B. Kong, C. Lu, X. J. Ma, X. M. Li and Y. C. Luo, *RSC Adv.*, 2013, 3, 6472.
34 M. C. Liu, L. B. Kong, C. Lu, X. M. Li, Y. C. Luo, L. Kang, *Mater. Lett.*, 2013, 94, 197.
35 H. N. Zhang, Y. J. Chen, W. W. Wang, G. H. Zhang, M. Zhuo, H. M. Zhang, T. Yang, Q. H. Li and T. H. Wang, *J. Mater. Chem. A*, 2013, 1, 8593.
36 W. Hong, J. Q. Wang, P. W. Gong, J. F. Sun, L. Y. Niu, Z. G. Yang, Z. F. Wang and S. R. Yang, *J. Power Sources*, 2014, 270, 516.
37 D. P. Cai, D. D. Wang, B. Liu, L. L. Wang, Y. Liu, H. Li, Y. R. Wang, Q. H. Li and T. H. Wang, *ACS Appl. Mater. Interfaces*, 2014, 6, 5050.
38 D. P. Cai, B. Liu, D. D. Wang, L. L. Wang, Y. Liu, H. Li, Y. R. Wang, Q. H. Li and T. H. Wang, *J. Mater. Chem. A*, 2014, 2, 4954.
39 X. Z. Yu , B. G. Lu and Z. Xu, *Adv. Mater.*, 2014, 26, 1044.
40 W. P. Sun, X. H. Rui, M. Ulaganathanc, S. Madhavia and Q. Y. Yan, *J. Power Sourse*, 2015, 295, 323.
41 J. Yan, Z. J. Fan, W. Sun, G. Q. Ning, T. Wei, Q. Zhang, R. F. Zhang, L. J. Zhi and F. Wei, *Adv. Funct. Mater.*, 2012, 22, 2632.
42 N. Padmanathan, K. M. Razeeb and S. Selladurai, *Ionics*, 2014, 20, 1323.
43 M. Q. Fan, B. Ren, L. Yu, D. L. Song, Q. Liu, J. Y. Liu, J. Wang, X. Y. Jing and L. H. Liu, *Electrochim. Acta*, 2015, 166, 168.
44 Z. X. Yin, S. Zhang, Y. J. Chen, P. Gao, C. L. Zhu, P. P. Yang and L. H. Qi, *J. Mater. Chem. A*, 2015, 3, 739.
45 D. P. Cai, D. D. Wang, B. Liu, Y. R. Wang, Y. Liu, L. L. Wang, H. Li, H. Huang, Q. H. Li and T. H, Wang, *ACS Appl. Mater. Interfaces*, 2013, 5, 12905.
46 M. Liu, L. Kong, C. Lu, X. Ma, X. Li, Y. Luo and L. Kang, *J. Mater. Chem. A*, 2013, 1, 1380.
47 H. Wan, J. Jiang, X. Ji, L. Miao, L. Zhang, K. Xu, H. Chen and Y. Ruan, *Mater. Lett.*, 2013, 108, 164.
48 L. Q. Mai, F. Yang, Y. L. Zhao, X. Xu, L. Xu and Y. Z. Luo, *Nat. Commun.*, 2011, 2, 381.
49 X. F. Lu, J. Lin, Z. X. Huang and G. R. Li, *Electrochim. Acta*, 2015, 161, 236.
50 B. Senthilkumar, D. Meyrick, Y. S. Lee and R. K. Selvan, *RSC Adv.*, 2013, **3**, 16542.

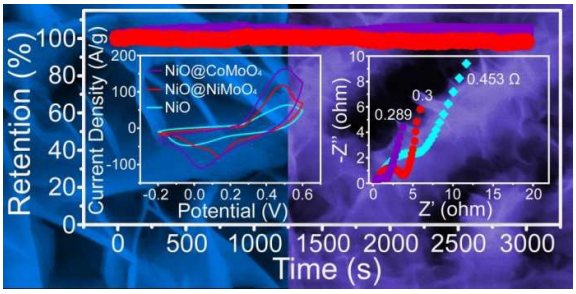

The hierarchical heterostructures of $NiO@MMoO_4$ (M = Co, Ni) nanosheet arrays electrode demonstrated remarkable electrochemical performance with high specific capacitance and predominant cycling stability.